Journal of Materials Science & Technology 147 (2023) 189–196

Contents lists available at ScienceDirect

Journal of Materials Science & Technology

journal homepage: www.elsevier.com/locate/jmst

Review Article

Chemical short-range orders in high-/medium-entropy alloys

Xiaolei Wu [a,b,*]

[a] State Key Laboratory of Nonlinear Mechanics, Institute of Mechanics, Chinese Academy of Science, Beijing 100190, China
[b] University of Chinese Academy of Science, Beijing 100049, China

ARTICLE INFO

Article history:
Received 11 July 2022
Revised 25 October 2022
Accepted 25 October 2022
Available online 27 December 2022

Keywords:
Chemical short-range order
Electron diffraction
Transmission electron microscopy
Structure motif
Chemical medium-range order
High-/medium-entropy alloys

ABSTRACT

High (or medium)-entropy alloys (H/MEAs) are complex concentrated solid solutions prone to develop the chemical short-range orders (CSROs), as an indispensable structural constituent to make H/MEAs essentially different from the traditional alloys. The CSROs are predicted to play roles in dislocation behaviors and mechanical properties. So far, the image of CSROs is built up by the theoretical modeling and computational simulations in terms of the conventional concept, i.e., the preference/avoidance of elemental species to satisfy the short-ranged ordering in the first and the next couple of nearest-neighbor atomic shells. In these simulated CSROs, however, the structural image is missing on the atomic scale, even though the lattice periodicity does not exist in the CSROs. Further, it is pending as to the issues if and what kind of CSRO may be formed in a specific H/MEA. All these are ascribed to the challenge of experimentally seeing the CSROs. Until recently, the breakthrough does not appear to convincingly identify the CSROs in the H/MEAs by using the state-of-the-art transmission electron microscope. To be specific, the electron diffractions provide solid evidence to doubtlessly ascertain CSROs. The structure motif of CSROs is then constructed, showing both the lattice structure and species ordering occupation, along with the stereoscopic topography of the CSRO. It is suggested that the CSROs, as the first landscape along the path of development of the local chemical ordering, offer one more route to substantially develop the ordered structure on the atomic scale in the H/MEAs, parallel to the existing grain-leveled microstructure. The findings of CSROs make a step forward to understand the CSROs-oriented relationship between the microstructure and mechanical properties. This review focuses on the recent progress mainly in the experimental aspects of the identification, structure motif, and mechanical stability in CSROs, along with the chemical medium-range orders as the growing CSROs.

1. Introduction

Chemical short-range orders (CSROs) have become a subject of ever-increasing concern in high-/medium-entropy alloys (H/MEAs) [1–4]. With the advent of convincing evidence, experimentally, to see CSROs for real [5,6], the significance manifests gradually in the following aspects. Firstly, the H/MEAs of multi-principal elements are apt to promote local chemical ordering (LCO) [7,8], which is usually not available in conventional alloys. The LCO potentially offers a new path to develop an additional microstructure, even metastable, with the CSROs as the incipient LCO [5,7]. Secondly, the theoretical modeling and computational simulations have shown the key roles of CSROs in the dynamics of defects [7,9,10], such as dislocation behaviors [7,11–15] and dislocation sources [16], along with stacking fault energy [17]. The CSROs are then closely related to plastic deformation [18–21], strengthening [22–25], strain hardening [26], and mechanical properties [27–32]. However, these roles of CSROs remain controversial so far [33]. The reason is the lack of adequate support particularly in the experiment as to the pending issues if and how CSROs interact with the gliding dislocations. Finally, the H/MEAs themselves are, in a sense, a kind of natural nanostructures [2,5]. CSROs stimulate to explore their effects on the typical microstructure-and-property relationship in the H/MEAs [6]. Here, the CSROs do not appear to be a new concept [34–36], at least superficially akin to the counterparts of usually a known intermetallic compound in most of the binary alloys [37–44]. Of particular curiosity are, here, the new meanings in the H/MEAs, along with the CSROs-tailored mechanical properties and performances [45,46].

* Correspondence to: State Key Laboratory of Nonlinear Mechanics, Institute of Mechanics, Chinese Academy of Science, Beijing 100190, China.
E-mail address: xlwu@imech.ac.cn

https://doi.org/10.1016/j.jmst.2022.10.070

An H/MEA of high configurational entropy is much more likely to form a single phase of a complex concentrated random solid solution [47,48]. Simultaneously, the enthalpy interaction inevitably exists due to the complex chemical interaction among constituent species [7]. The formation enthalpy may become dominant in free energy to drive the high entropy solid solution metastable. The local chemical environment is thus induced by the low and even negative enthalpy. In other words, the enthalpy-driven heterogeneities appear on the atomic scale to some degree/extent [7,10]. One is the concentration waves [49] characterized by the pronounced inhomogeneous compositional fluctuation of chemical species [50–58]. The other is the LCO [7], which develops along the route starting from CSROs [5,6], followed probably by the chemical medium-range orders (CMROs) [59]. In other words, CSROs are the incipient LCO, while the CMROs are growing CSROs [59]. In addition, the nano-precipitation of ordered intermetallic compounds often exists in the H/MEAs, e.g., $L1_2$ and B2, etc, by the addition of Ti and Al, etc [60,61]. Yet, the embryonic stage of these compounds is not a true sense of the concerned CSROs.

The H/MEAs would most likely develop parallel microstructures of two kinds. One is the grain-leveled microstructure, while the other is the spontaneous LCO on the atomic scale. The H/MEAs are therefore considered as a trans-scale heterostructure [62,63], with the constituent phases spanning several orders of magnitude in sizes from the sub-nanometer CSROs to common grains. This makes the H/MEAs markedly differ from the conventional alloys. In other words, the LCO, together with the concentration waves, is added in consideration of the common microstructure-and-property relationship. Incidentally, the grained microstructures will evolve and plastically deform in the H/MEAs in a way almost consistent with that in conventional alloys [64], including dislocation behavior [65], deformation twinning [66], and phase transformation, etc [67].

The effect of CSROs on plastic deformation remains quite elusive, especially in the experiment so far [5–7]. The tendentious view is the analogy of CSROs to the nano-precipitates. The smaller particles in size, the larger resistance will be to the slip of dislocations. This is really true for the precipitates [68,69], while a similar expectation is reasonable as long as the CSROs are mechanically stable [5,59]. Recently, several experimental results, almost all lacing with the assumptions and inferences, indicate the effect of CSROs on the strengthening [70–78], strength and ductility [79–81], and other performances [82–84]. Further, the CSROs-oriented strategy is suggested for the advanced H/MEA designs to realize the superior strength-and-ductility synergy [1,2,5,85].

The CSROs are the first and primary scenery to appear on the chain of LCO in the H/MEAs. CSROs build up the blocks which expand and grow later in one, two, or three dimensions. For this reason, the CSROs cannot be emphasized enough as the basis of the subsequent evolution of LCO. The first challenge is, however, to convincingly identify the CSROs [5,59]. In this review article, several aspects are analyzed and discussed regarding the recognition of CSROs and CMROs, along with their structure motif and mechanical stability, shedding light on the path for an in-depth understanding of the intrinsic structural features.

2. TEM identification of CSROs

The usual methods to experimentally identify CSROs include X-ray/neutron diffraction [86,87], atom probe tomography [88,89], transmission electron microscopy (TEM) [5,6,42–44], etc. Thereinto, the TEM technique may simultaneously show the three essential ingredients to exactly describe a CSRO [5,90,91]. The first, actually as the basis of the latter two, is the electron diffraction, showing an identified signal with regard to the crystal structure of the CSRO, only without lattice periodicity yet [5,59]. The second is the energy-filtered dark-field image to truly see the CSROs [5,6]. The third is the elemental analysis map to determine the spacial order occupation of constituent species in the crystal lattice of a CSRO [5,90,91]. Yet, the difficulty unexpectedly arises at first in electron diffraction, especially in H/MEAs. It is unacquainted as to exactly under which zone axis, one and maybe more, the extra superlattice scattering from the CSROs appears in the electron diffraction. This is ascribed to the uncertainty of CSRO lattices in the H/MEAs. However, this wasn't supposed to be a difficulty in the conventional binary alloys [41,43,92], where the CSRO is usually fixed already as a known crystal structure of an ordered long-range intermetallics compound.

Recently, TEM observations of CSROs have been conducted in several representative face-centered cubics (fcc)-structured H/MEAs, including CrCoNi [90], VCoNi [5], and $Al_{9.5}$CrCoNi [59] MEA, along with $Fe_{50}Mn_{30}Co_{10}Cr_{10}$ HEA [91]. The main concerns are as follows. The CrCoNi, often as a prototypical fcc MEA, motivated the earliest experimental study of CSROs [6,90]. Three species are much close in the periodic table of elements and their electronegativity, such that the enthalpy of mixing of this alloy may not be sufficiently large in magnitude to drive the pronounced and widespread chemical ordering/clustering. Indeed, over the entire range of temperatures and compositions, the CrCoNi does not show the equilibrium intermetallic compounds [6]. One naturally wonders if the CSROs can be developed in such a completely soluble alloy with the composition in the center of phase diagram, simultaneously without the chemically ordered metastable state to be predicted as a potential candidate/reference. Furthermore, the constituent species are similar in atomic scattering factor such that the extra reflections from CSROs, if with a moderate volume density, would be rather low in diffraction intensity. Secondly, both the VCoNi [93] and $Al_{9.5}$CrCoNi [94] are the same type of dual-phase MEAs. Either V or Al locally induces the low (negative) enthalpy of mixing so as to increase the tendency for the CSROs. By contrast to CrCoNi, the intermetallic compounds of either $L1_2$ or B2, respectively, are formed in both alloys. If CSROs do develop, it is curious if and what kind of CSRO would emerge, instead of the embryonic $L1_2$ and B2. Finally, $Fe_{50}Mn_{30}Co_{10}Cr_{10}$ is a quaternary and non-equiatomic HEA [67], with the initial dual phases of both the fcc and close-packed hexagonal (hcp) structures, without any ordered compounds to form in both phases. In such a high-entropy case, exactly what kind of CSRO would be developed, and to what extent are questions that have not been convincingly answered thus far.

2.1. Characteristic diffuse scattering by CSROs

Recently, a full suite of clear-cut experiments in an aberration-corrected TEM has been suggested to irrefutably identify the CSROs in H/MEAs [5,90,91]. Firstly, by means of the most common selected-area electron diffraction (SAED) as well as the micron-beam diffraction and lattice-image-based fast Fourier transform (FFT), any diffraction pattern of these three kinds may act independently as the criterion and/or signal of CSROs under an appropriate zone axis. Secondly, the CSROs may be seen clearly by both the energy-filtered high-angle annular dark field (HAADF)-scanning-TEM (STEM) and inverse-FFT (IFFT) imaging. Finally, the atomic-scale chemical composition can be determined to show the ordered species occupation according to the energy dispersive spectroscopy (EDS) mapping.

The first step is critical to acquire the SAED pattern. The CSROs induce the extra superlattice scattering to manifest in the diffuse disks in reciprocal space, with the sizes substantially larger than those of Bragg spots by host lattice [5,90,91]. This diffraction feature indicates exclusively that the tiny CSRO entities exist in real space [95,96]. This corollary is derived from the rule-

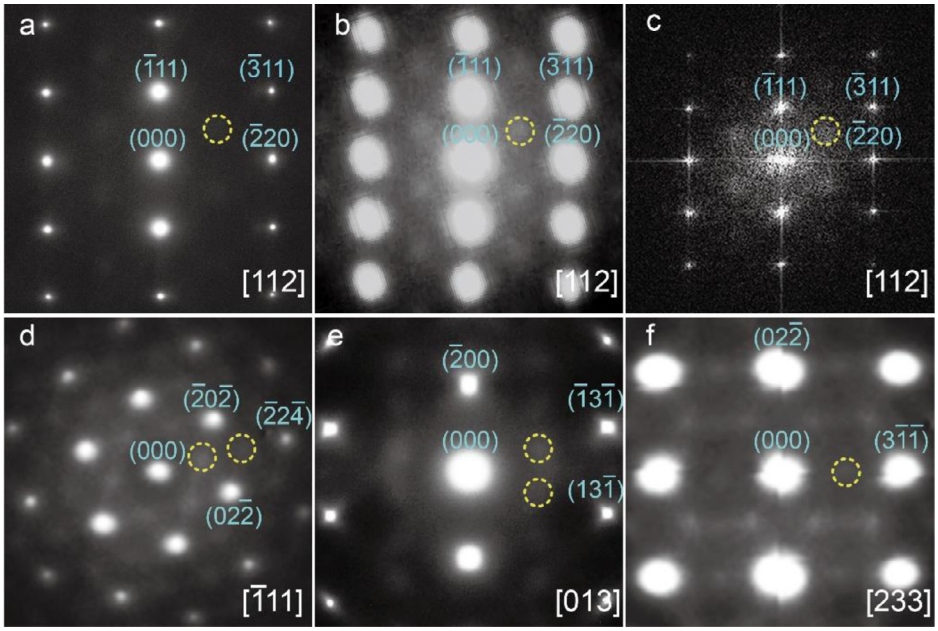

Fig. 1. Characteristic diffuse scattering by CSROs in the SAED patterns under varying high index zone axes (z.a.). (a, b, c) SAED, nano-beam diffraction, and FFT patterns, all under [112] z.a. [5]. (d, e, f) SAED patterns, respectively, under the [111] [97], [013], and [233] z.a.. All patterns are indexed, with one or two yellow circles indicating diffused scattering by CSROs.

of-shape factor between real and reciprocal space, i.e., 'small becomes large' and vice versa [95]. In other words, diffuse scattering is the hallmark feature of CSROs due to their small sizes and varying contents inside the column of TEM film for diffraction testing. However, challenges arise in the SAED pattern from the CSROs in H/MEAs. On one hand, the diffraction intensity relies on the crystallographic orientations. The extra scattering by the CSROs will become highly diffuse and extremely weak in intensity due to the moderate volume density and small sizes typically below one nanometer. This makes it much more difficult for CSROs to yield the recognizable scattering in the diffraction pattern. On the other hand, the CSROs are strongly asymmetric in the spatial three-dimension (3D) shapes especially at their initial stage [97]. As such, the extra scattering is usually visible only in one incident direction, while becomes much weaker and even disappears in others even though all are a family of the same orientation, not to mention that this is more likely to happen under the different zone axis [5,97].

The methods of electron diffraction of three kinds are reported to successfully catch sight of the diffuse scattering of CSROs in the electron diffraction patterns [5,97]. The first is the SAED pattern, especially under a few high-index zone axes, e.g., the [112], [013], [111], and [233] zone axes, as shown in Fig. 1 [5,97]. Under these zone axes, the extra scattering induced by CSROs appears all in the form of diffuse disks, and one is circled in yellow. These diffuse scattering lines up at the $\frac{1}{2}\{\bar{3}11\}$ positions of host fcc lattice under the [112], [013], and [2̄33] zone axis, as shown in Fig. 1(a, e, f), while at the $\frac{1}{3}\{\bar{4}22\}$ and $\frac{2}{3}\{\bar{4}22\}$ positions under the [111] zone axis, as shown in Fig. 1(d). The second is the nano-beam diffraction, as shown in Fig. 1(b) still under the [112] zone axis, to significantly increase the diffraction intensity of extra scattering by substantially improving the signal-to-noise ratio. The extra scattering at the $\frac{1}{2}\{\bar{3}11\}$ positions increases in intensity. The third method is the FFT pattern based on high-resolution TEM lattice imaging, as shown in Fig. 1(c). The diffuse scattering is visible at the $\frac{1}{2}\{\bar{3}11\}$ positions under the [112] zone axis. In a word, diffuse disks in reciprocal space are evidence for the presence of small CSRO entities in real space [5,90,91,97]. In addition, the CSROs do not show their signature diffuse scattering in the SAED patterns under the routinely used [109] beam direction [5,97].

Caution is needed, however, as to the electron diffraction used for the recognition of CSROs. Firstly, extra reflections, usually in the form of spots, small in size but rather sharp in intensity, are often mistakenly assumed to come from the CSROs in either the H/MEAs or conventional alloys. The sharp spots are usually indicative of the long-range periodicity of a crystal lattice based on the mutual relationship between real and reciprocal space for a crystal [95]. Secondly, the extra superlattice reflections are sometimes not so diffuse after all. This is possibly an ordered region that has extended to well above 1 nm, beyond the size realm of CSROs. Namely, the chemical ordering has evolved and/or expanded to a spatial extent that already corresponds to a long-range order across the regions of at least a few nanometers in one or more dimensions. The side-by-side observation is thus suggested by either dark-field imaging or chemical analysis to determine the sizes of these tiny entities. In any case, however, the highly diffuse scattering is the basic criterion to identify CSROs. Thirdly, the CSROs may be so dilute and diverse in shape in some cases that they may escape the detection altogether with the TEM techniques today.

The CSROs are often confused also with an equilibrium/metastable intermetallic compound. Their precipitates will go through various stages, sizes, and morphology in both the conventional alloys and H/MEAs [38,42,98,99]. In other words, the tiny nano-precipitates are often wrongly guessed as the LCOs. Meanwhile, the H/MEAs are metastable and prone to either compositional decomposition or phase separation. This is an entirely different question from CSROs inherent in the as-prepared single-phase solution of H/MEAs. The doubt is ascribed to the constituent species in these precipitates where the ordering configurations have not been deciphered in detail. This emphasizes the importance of experimental evidence of two kinds to ascertain the CSROs simultaneously. One is the diffraction, while the other is the atomic ordering occupation. The CSROs show, in fact, the chemical ordering which can be entirely different from that found in any known compounds [5,59]. This is the focus of attention. For example, the CSROs are of the $L1_1$-type structure motif [97],

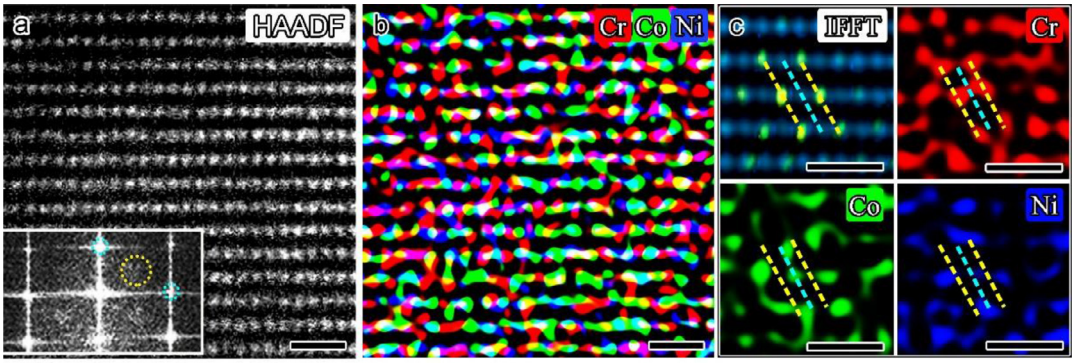

Fig. 2. Element distribution in CSRO of CrCoNi. (a) HAADF lattice image of fcc phase with the [112] z.a.. Inset: FFT pattern showing CSROs-induced diffuse scattering at $\frac{1}{2}\{\bar{3}11\}$ positions (one is labeled by the yellow circle). (b) Corresponding EDS map. (c) IFFT of CSRO region (upper-left) and EDS maps of Cr, Co, and Ni, respectively. All dashed lines mark the $(\bar{3}11)$ planes. Yellow: Cr-enriched, Blue: Co-/Ni- enriched. All scale bars are 0.5 nm in length.

different from the intermetallic compound of $L1_2$ in VCoNi MEA [5] and of B2 in $Al_{9.5}$CrCoNi MEA [59].

2.2. Chemical information of CSROs

The chemical information of species occupation is indispensable for the full understanding of the atomic structure of CSROs. As to a CSRO, the ordering means the occupancy of constituent species on certain lattice planes/sites in the nearest-neighbor environment. Fig. 2(a) is an HAADF lattice image of the fcc phase in CrCoNi under the [112] z.a. [90]. Inset is the corresponding FFT pattern showing the extra diffuse reflections by the CSROs (one is labeled by a yellow circle) at $\frac{1}{2}\{\bar{3}11\}$ positions. Fig. 2(b) is the EDS mapping showing the element distribution. Fig. 2(c) is the IFFT of a specific CSRO region (upper-left) and corresponding EDS maps of Cr, Co, and Ni, respectively, for this CSRO. All dashed lines mark the $(\bar{3}11)$ planes intersecting the (111) plane in plan view. The dashed yellow lines indicate Cr-enriched, while the blue lines are Co-/Ni-enriched. To be specific, in Cr-map, two Cr-enriched $(\bar{3}11)$ planes (dashed yellow lines, across red spots) sandwich one Cr-depleted $(\bar{3}11)$ plane (in either Co or Ni map, both under the blue line). For this reason, a CSRO consists of a (Co, Ni)-enriched plane sandwiched by two Cr-enriched planes [90].

2.3. Structure motif of CSROs

The structure motif is, in principle, a 3-D unit cell on the atomic scale to depict a CSRO from two aspects: atomic configuration and species ordering occupation [97]. The CSRO motif may help an in-depth understanding of the nucleation and later growth of CSROs, along with the mutual relationship with the host lattice. Particularly, the spatial 3-D form of the CSRO can be derived also as an added benefit. Recently, the method has been developed to establish the 3-D structure motif of CSROs in terms of both the mutual relationship and correspondence of crystal lattice between the real and reciprocal space by using the electron diffractions under the multiple zone axes, refer to Ref. [97] for details. Here, VCoNi is taken as an example, as shown in Fig. 3. Firstly, based on the SAED pattern under a [112] zone axis, as shown in Fig. 3(a-1), and the position of CSRO in host lattice, as shown in Fig. 3(a-2), the two-dimensional (2-D) CSRO model is established in the [111] direction, as shown in Fig. 3(a-3). Namely, V atoms (spheres in pink) occupy the vertices of the unit cell, while both Co and Ni atoms (in yellow) locate in between [97]. Secondly, with the help of the SAED pattern under the [111] zone axis, as shown in Fig. 3(b-1), the extra diffuse scattering by CSROs is visible at the positions of $\frac{1}{3}\{\bar{4}22\}$ and $\frac{2}{3}\{\bar{4}22\}$ of host base, one is circled in pink. The diffraction pattern is then simulated, as shown in Fig. 3(b-2), where the $\{\bar{2}02\}$ reflections, labeled by $\times$ s in pink, are forbidden for CSROs, in contrast to the clearly visible scattering by CSROs at the positions of $\frac{1}{3}\{\bar{4}22\}$. The reason is that the diffraction pattern was simulated under the assumption of the long-range, disordered arrangement of atoms, while CSROs are chemically ordered, such that the CSROs-induced scattering will not satisfy the strict extinction law to make the diffraction deviate from the theoretical extinction. The 2-D model is then established under the [111] zone axis, Fig. 3(b-3), where the hexagon (dash line in pink) is the periodic, minimum unit cell. Thirdly, under the [011] zone axis in Fig. 3(c-1), the scattering by CSROs is not available. Yet, the CSROs can be still found in the host lattice in terms of CSRO-induced strain distribution in Fig. 3(c-2), by means of the atomic-scale geometric phase analysis (GPA) [5]. The 2-D model is thus established with the [109] zone axis in Fig. 3(c-3). Finally, the CSRO motif, i.e., 3-D unit cell, is reconstructed, as shown in Fig. 3(d), based on the above three 2-D models, demonstrating full information of both lattice structure and order occupation of three elements. Interestingly, the 3-D unit cell of CSROs is determined as $L1_1$ [97], with $a = 0.747$ nm and $\gamma = 89.9°$. In the motif, the atomic occupation is re-arranged in the CSRO as a result of the chemical order, relative to the host fcc lattice.

The spatial 3-D morphology of CSRO looks like a flat cuboid based on the 3-D unit cell, outlined in pink in Fig. 3(e). It follows that to see the CSROs depend on the incident direction, i.e., the zone axis relative to the host lattice. In other words, more CSROs will be seen if viewed from the [112] zone axis, parallel to the major axis of CSROs. However, this does not necessarily mean that it is true under all <112> zone axes. For example, both [121] and [211] zone axes deviate an angle of 33.6° with the major axis of CSROs. This leads to a decrease in the proportion of CSROs inside the special column for diffraction imaging in the TEM thin film. The diffraction intensity by CSROs will become weak such that it is hard to distinguish them from the noised background [5,6]. By contrast, the [109] zone axis is parallel to the minor axis of CSROs. Accordingly, the diffraction intensity is much weak by comparison with that under the [112] zone axis. This is the reason that it is hard to see extra scattering along the [109] zone axis. The same is true for the [111] zone axis. Simply to say, whether or not the extra diffuse diffraction by CSROs appears will depend on the spatial shape of CSROs and the orientation relationship between CSRO and zone axis, along with the thickness of TEM film for CSRO observations.

The consistent features of CSROs have been shown in several H/MEAs [5,59,90,91]. Firstly, if viewed under the [111] zone axis, the extra scattering by CSROs always occurs at the $\frac{1}{2}$[311] locations in the diffraction pattern. Secondly, CSROs have an identical preferential occupancy of species. To be specific, two *M*-enriched

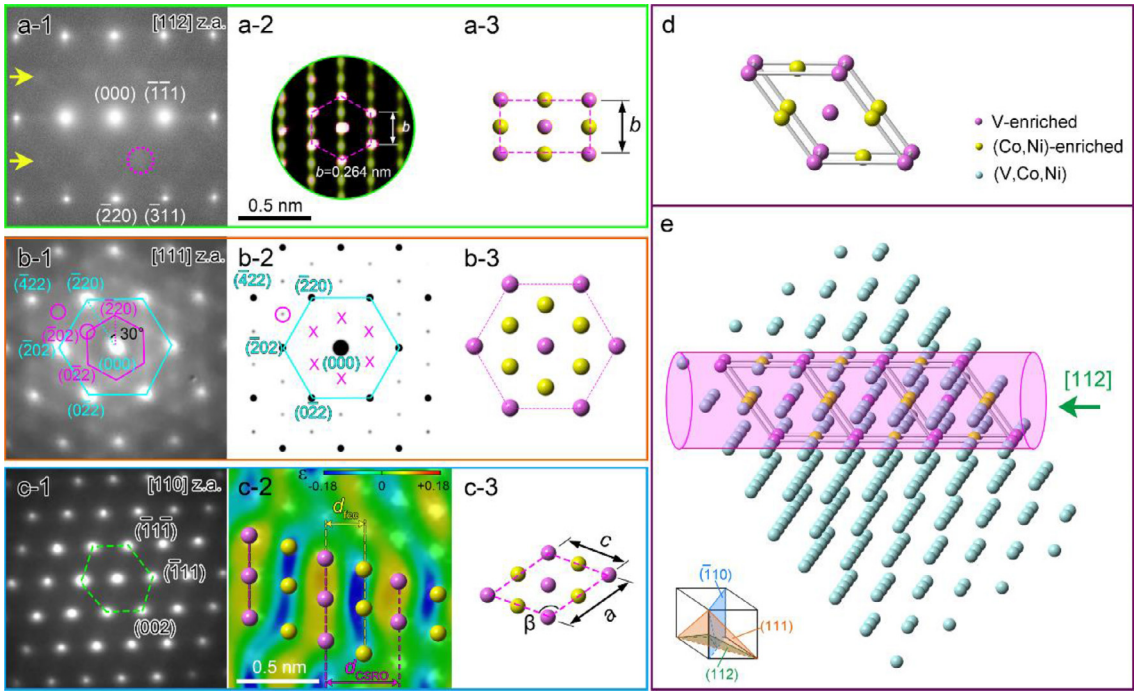

Fig. 3. 3-D structure motif of CSROs. (a) Electron diffraction of CSROs under [112] z.a.. (a-1) SEAD pattern. (a-2) Merged FFT and inverse FFT pattern. (a-3) 2-D model. (b) Electron diffraction of CSROs under [111] z.a. (b-1) Nano-beam diffraction pattern. (b-2) Simulated diffraction pattern. (b-3) 2-D model. (c) Electron diffraction of CSROs under [109] z.a.. (c-1) Nano-beam diffraction pattern. (c-2) GPA map. (c-3) 2-D model. (d) 3-D unit cell. (e) 3-D morphology.

{311} planes sandwich one *M*-depleted {311} plane, here *M* refers to a body-centered cubic (bcc) element, e.g., V in VCoNi [5] and Cr in CrCoNi [90]. It is thus derived that CSROs in all these H/MEAs unexpectedly exhibit the same $L1_1$-type motif, along with a similar spatial shape. However, it is so far inquisitive for the reason of the same motif of CSROs to appear in these H/MEAs of obviously different species. By the way, the $L1_1$-type motif is also determined for the CSROs in the high-Mn steel [100]. Finally, the 3-D motif makes a step forward to provide information on both the structure and occupation in CSROs, relative to simulated CSROs constructed by the computational modeling and simulations based on conventional definition [101–114].

3. Chemical medium-range order (CMRO)

CMROs are indispensable intermediate links during the development of LCO in the H/MEAs [59,97,98]. The CMROs are the next-level LCO in contrast to CSROs as the incipient LCO [5,59]. The size range is defined within 1–5 nm, even a little bit arbitrary. Accordingly, the CMROs will exhibit the defining lattice periodicity. In this sense, the CMROs are a significant mark of the structural gene which helps to understand the evolution of LCO. The issues are unclear as to firstly, if and what kind of CMRO will be generated and secondly if CMROs are mechanically stable during tensile deformation.

The first thing to address is the iconic electron diffraction to identify the CMROs [59], and the same problem ever met for CSROs. In the fcc phase of $Al_{9.5}$CrCoNi MEA, the extra superlattice scattering appears in the SAED pattern under two high-index [112] and [013] zone axes and in the nano-beam diffraction, Fig. 4(a–c). The signature scattering by CMROs is in the form of spots of concentrated diffraction. These spots locate at the $\frac{1}{2}[\bar{3}11]$ positions of the fcc lattice, as indicated by arrows and one is circled in yellow. The spots are much small in size, different from the highly diffuse disks of large diameter by CSROs [5,89]. Further, these spots are even much weaker in intensity than sharp spots from the host lattice. Based on the definitive relationship and correspondence between real and reciprocal space [95], these spots are ascribed to the CMRO entities: they are beyond CSROs in size, but still much tiny, and already have the lattice periodicity. In fact, most CMRO entities show a size range of several nanometers, as shown in Fig. 4(d), comparable to the nano-precipitates in conventional alloys and H/MEAs. Interestingly, both CMROs (>1 nm) and CSROs are co-existent. The CMRO entities show sizes >1 nm, with an average size ($\bar{d}$) of 1.6 nm, which is larger than that of 0.6 nm for CSROs. Further, both CSROs and CMROs have a consistent chemical order. Fig. 4(e) is the HAADF lattice image, with the inset showing the FFT pattern. Fig. 4(f) is the IFFT image, showing a CMRO region. Fig. 4(g, h) are EDS maps. As to Cr at the upper-left corners in both cases, both the CSROs and CMROs show a similar feature of species occupation. To be specific, two Cr-enriched $(\bar{3}11)$ planes (dashed white lines, across green spots) sandwich one Cr-depleted $(\bar{3}11)$ plane under yellow line. This is also consistent with species occupation in other H/MEAs previously reported [5,90,91]. It, therefore, follows that the CMROs are growing CSROs.

Several comparisons are made between CMROs and CSROs to shed light on the path of LCO development. Firstly, the chemical ordering in CMROs is in full accord with that in CSROs: the alternating {311} planes with the preference for unlike pairs and avoidance of unlike pairs. Both holds for the present CMROs and all other CSROs investigated so far. Second, the 3-D structure motif in the present CMROs is similar to that of CSROs based on the consistent diffraction patterns under various diffraction zone axes. The lattice structure is $L1_1$, instead of the B2 compound existing already as the second phase in the fcc matrix.

4. Mechanical stability of CSROs and CMROs

Whether or not the CSROs are mechanically stable is a matter of long unknown. There exists at least one view that the CSROs may be destroyed during plastic deformation with a fairly high probability. This is due to the moving dislocations apt to destroy the

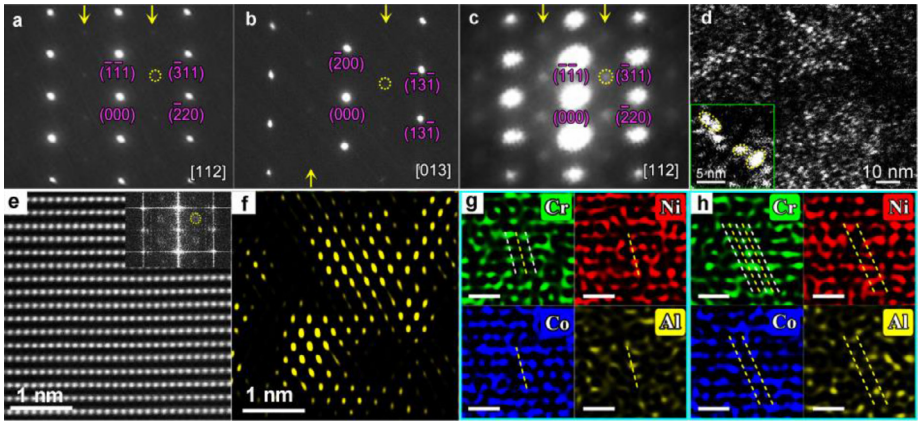

Fig. 4. CMROs in $Al_{9.5}CrCoNi$ MEA. (a, b) Selected-area electron diffraction patterns under the [112] and [013] z.a.. (c) Nano-beam diffraction. [112] z.a. Yellow arrows in (a–c): arrays of extra scattering. Yellow circles: extra reflection. (d) Dark-field image taken by extra reflections in (a), showing CMRO entities. Inset: close-up view of several CMROs. (e) HAADF lattice image. [112] z.a. Inset: FFT pattern showing extra scattering at $\frac{1}{2}\{\bar{3}11\}$ positions (one is labeled by a yellow circle). (f) IFFT of CMRO region. (g, h) EDS maps showing the elemental distribution of Cr, Ni, Co, and Al, respectively, in CSRO (g) and CMRO (h). All dashed lines mark the $(\bar{3}11)$ planes. Yellow: Cr-enriched, blue: Co-/Ni- enriched. Scale bar in (g, h): 0.5 nm.

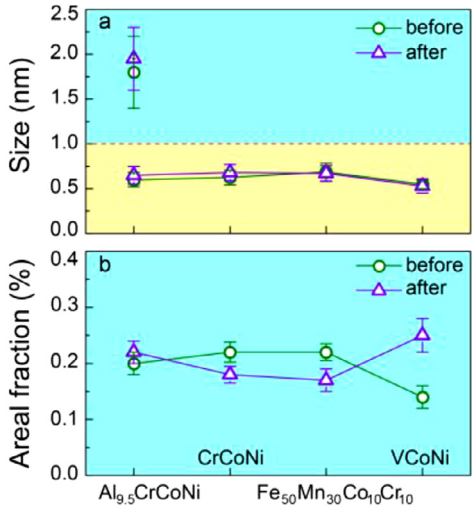

Fig. 5. Mechanical stability of both CSROs and CMROs. (a, b) Average size and areal fraction in H/MEAs of four kinds before and after tensile deformation.

chemical ordering in the CSROs of small sizes. However, the CSROs are of the lattice structure already, e.g., $L1_1$-type motif, even without the long-range lattice periodicity yet. This will induce obstacles in regard to both the thermodynamic energy and dynamic diffusion, which makes the CSROs stable to varying degrees upon applied loading.

The CSROs, along with CMROs, have indeed shown mechanical stability during tensile deformation in Fig. 5(a). There is no obvious change in the sizes of CSROs and CMROs before and after tensile deformation. Simultaneously, the areal fraction (F_{area}) of both CMROs and CMROs entities is ~20% before tensile deformation in Fig. 5(b), which is almost unchangeable after tensile deformation, except for VCoNi showing a little bit of increase [5].

5. CSROs-oriented plastic deformation

Strength and ductility have long been a pair of ineradicable paradoxes in traditional metals and alloys [115,116]. Similarly, the strength-and-ductility trade-off arises in H/MEAs [64,67,85]. Ductility is ascribed to strain hardening, which is mediated by the dislocation of plasticity during plastic deformation to induce the generation, multiplication, and interaction of dislocations. To further reinforce strain hardening, microstructure-oriented strategies are applied for example to fill the grain interior with the sub-structures of varying kinds, e.g., nano-twins [66], precipitates [60,61], and second phases [94], etc. Thereinto, the most efficient is precipitation by the elaborate design of elemental species on basis of the H/MEAs [60,61,79,80], already as the recipe in the state-of-the-art ultra-high strength steels [117]. It is expected that the stable CSROs will interact with gliding dislocations [5,7]. Therefore, both strengthening and strain hardening are highly expected due to much small sizes and spacing of CSROs. Unfortunately, the evidence is rare experimentally in the interaction between CSROs and dislocations. The strengthening effect and strain hardening claimed by the CSROs are a little bit untenable due to the influence of many microstructural factors. The main difficulty lies in the impossibility of simultaneously seeing both the CSROs and dislocations.

6. Conclusive remarks and perspectives

The chemical short-range orders have been gradually accepted as an inevitable exist at least in several typical fcc-structured H/MEAs, which are either single phase, e.g., CrCoNi, or dual phases, e.g., VCoNi and $Al_{9.5}CrCoNi$, already having the intermetallic compound $L1_2$ and B2. The medium-range orders are the projected extension from short-range orders in the line of local chemical ordering. Both short- and medium-range orders are considered iconic constituents inherent in the microstructure. Three essential ingredients are emphasized for the identification of the short-/medium range orders, including electron diffraction, dark-field imaging, and elemental occupation. The electron diffractions of three kinds are available to convincingly ascertain the ordering, including the selected-area electron diffraction, fast Fourier transform, and nano-beam electron diffraction. The high-index zone axes of electron diffraction are suggestive, such as [112], [013], and [111] zone axes. The characteristic extra superlattice scattering is the diffuse disks of large sizes and small, weak spots, respectively, for the short- and medium-range orders. Particularly, the existing experimental results make the progress of a few steps. First, the ordering, especially short-ranged, is truly seen. Second, the short-range ordering is of the structural feature on atomic-scale due to the ordered species occupation, i.e., a $L1_1$-type motif. Third, the short-range ordering has a 3-D shape, e.g., the flat cuboid. Importantly, both the short- and medium-range orders form with a new crystal structure, different from the chemical order of known intermetallic phases.

The evidence of chemical short-range orders, experimentally even less than more theoretical and computational simulations, demonstrates the presence of local chemical order as an additional path to the microstructural development in the H/MEAs. This brings about the challenge to understand the microstructure-and-property relationship but at the same time, also creates an opportunity for advanced properties and performances over conventional alloys. From a general perspective, it is anticipated that mechanically stable short-/medium-range orders will enhance mechanical properties. The large-size orders are much likely more effective to reinforce the natural interaction with dislocations upon straining. For this reason, chemical ordering, as a potential strategy, offers a new knob to tailor the macroscopic properties in the H/MEAs. It is further suggested that the H/MEAs can be regarded as an innate nano-structure because of widespread short-/medium-range orders. In this sense, the CSRO-oriented design is advocated for the effect of CSROs related to structural type, stability, contents, etc., in a specific H/MEA.

Acknowledgments

This work was financially supported by the National Key Research and Development Program of the Ministry of Science and Technology of China (No. 2019YFA0209902), the National Natural Science Foundation of China (Nos. 11998102, 11972350, and 11790293), and the Strategic Priority Research Program of the Chinese Academy of Sciences (No. XDB22040503).

References

[1] Y. Wu, F. Zhang, X.Y. Yuan, H.L. Huang, X.C. Wen, Y.H. Wang, M.Y. Zhang, H.H. Wu, X.J. Liu, H. Wang, S.H. Jiang, Z.P. Lu, J. Mater. Sci. Technol. 62 (2021) 214–220.
[2] R.P. Zhang, Y.J. Chen, Y. Fang, Q. Yu, MRS Bull. 47 (2022) 186–193.
[3] J. Ding, Z.J. Wang, Acta Metall. Sin. 57 (2021) 413–424.
[4] Y.Q. Bu, H.T. Wang, Adv. Mech. Eng. 51 (2021) 915–919.
[5] X.F. Chen, Q. Wang, Z.Y. Cheng, M.L. Zhu, H. Zhou, P. Jiang, L.L. Zhou, Q.Q. Xue, F.P. Yuan, J. Zhu, X.L. Wu, E. Ma, Nature 592 (2021) 712–716.
[6] R.P. Zhang, S.T. Zhao, J. Ding, Y. Chong, T. Jia, C. Ophus, M. Asta, R.O. Ritchie, A.M. Minor, Nature 581 (2020) 283–287.
[7] Q.J. Li, H. Sheng, E. Ma, Nat. Commun. 10 (2019) 3563.
[8] J.M. Cowley, Phys. Rev. 77 (1950) 669–675.
[9] S.J. Zhao, Phys. Rev. Mater. 5 (2021) 103604.
[10] S. Chen, Z.H. Aitken, S. Pattamatta, Z.X. Wu, Z.G. Yu, R. Banerjee, D.J. Srolovitz, P.K. Liaw, Y.W. Zhang, Acta Mater. 206 (2021) 116638.
[11] S. Yin, Y. Zuo, A. Abu-Odeh, H. Zheng, X.G. Li, J. Ding, S.P. Ong, M. Asta, R.O. Ritchie, Nat. Commun. 12 (2021) 4873.
[12] M. Sudmanns, J.A. El-Awady, Acta Mater. 220 (2021) 117307.
[13] X.Y. Wang, F. Maresca, P.H. Cao, Acta Mater. 234 (2022) 118022.
[14] S.C. Dai, Z.C. Xie, Y.J. Wang, Int. J. Plast. 149 (2022) 103155.
[15] S.H. Ma, J. Zhang, B. Xu, Y.X. Xiong, W. Shao, S.J. Zhao, J. Alloy. Compd. 911 (2022) 165144.
[16] L.T. Smith, Y.Q. Su, S.Z. Xu, A. Hunter, I.J. Beyerlein, Int. J. Plast. 134 (2020) 102850.
[17] J. Ding, Q. Yu, M. Asta, R.O. Ritchie, Proc. Natl. Acad. Sci. U. S. A. 115 (2018) 8919–8924.
[18] W.R. Jian, Z.C. Xie, S.Z. Xu, Y.Q. Su, X.H. Yao, I.J. Beyerlein, Acta Mater. 1100 (2020) 352–369.
[19] L. Guo, J. Gu, X. Gong, K. Li, S. Ni, Y. Liu, M. Song, Micron 126 (2019) 102739.
[20] M.L. Ali, S. Shinzato, V. Wang, Z.Q. Shen, J.P. Du, S. Ogata, Mater. Trans. 61 (2020) 605–609.
[21] Y. Ma, Q. Wang, C.L. Li, L.J. Santodonato, M. Feygenson, C. Dong, P.K. Liaw, Scr. Mater. 144 (2018) 64–68.
[22] S. Nag, W.A. Curtin, Acta Mater. 200 (2020) 659–673.
[23] E. Antillon, C. Woodward, S.I. Rao, B. Akdim, T.A. Parthasarathy, Acta Mater. 190 (2020) 29–42.
[24] E. Antillon, C. Woodward, S.I. Rao, B. Akdim, Acta Mater. 215 (2021) 117012.
[25] W.Q. Cheng, F.P. Yuan, X.L. Wu, Front. Mater. 8 (2021) 767795.
[26] F. He, S.L. Wei, J.L. Cann, Z.J. Wang, J.C. Wang, C.C. Tasan, Acta Mater. 220 (2021) 117314.
[27] S. Dasari, A. Jagetia, A. Sharma, M.S.K.K.Y. Nartu, V. Soni, B. Gwalani, S. Gorsse, R. Banerjee, Acta Mater. 212 (2021) 116938.
[28] S. Chen, Z.H. Aitken, S. Pattamatta, Z.X. Wu, Z.G. Yu, D.J. Srolovitz, P.K. Liaw, Y.W. Zhang, Nat. Commun. 12 (2021) 4953.
[29] A. Sharma, P. Singh, D.D. Johnson, P.K. Liaw, G. Balasubramanian, Sci. Rep. 6 (2016) 31028.
[30] X.T. Liu, H.Y. Zhao, H.S. Ding, D.Y. Lin, F.Y. Tian, Appl. Phys. Lett. 119 (2022) 131904.
[31] Y. Liu, G.P. Zheng, M. Li, J. Alloy. Compd. 843 (2020) 156060.
[32] H.G. Liu, S. Tang, Y.Z. Ma, W.S. Liu, C.P. Liang, Scr. Mater. 204 (2021) 114136.
[33] B. Yin, S. Yoshida, N. Tsuji, W.A. Curtin, Nat. Commun. 11 (2020) 2507.
[34] J.B. Cohen, M.E. Fine, J. Phys. Radium 23 (1962) 749–762.
[35] V.I. Iveronova, A.A. Katsne'son, Sov. Phys. J. 19 (1976) 1002–1011.
[36] M.A. Krivoglaz, Phys. Met. 6 (1985) 1–53.
[37] S. Matsuo, L.M. Clarebrough, Acta Metall. 11 (1963) 1195–1206.
[38] P.R. Okamoto, G. Thomas, Acta Metall. 19 (1971) 825–841.
[39] S. Hata, D. Shindo, T. Mitate, N. Kuwano, S. Matsumura, K. Oki, Micron 31 (2000) 533–538.
[40] A. Marucco, B. Nath, J. Mater. Sci. 23 (1988) 2107–2114.
[41] W. Garlipp, M. Cilense, C.R.S. Beatrice, Scr. Metall. Mater. 29 (1993) 1035–1037.
[42] N. Kuwano, N. Chiwata, K. Oki, Bull. Mat. Sci. 22 (1999) 697–700.
[43] R.P. Zhang, S.T. Zhao, C. Ophus, Y. Deng, S.J. Vachhani, B. Ozdol, R. Traylor, K.C. Bustillo, J.W.M. Jr, D.C. Chrzan, M. Asta, A.M. Minor, Sci. Adv. 5 (2019) eaax2799.
[44] Z.Z. Song, R.M. Niu, X.Y. Cui, E.V. Bobruk, M. Murashkin, N.A. Enikeev, R.Z. Valiev, S.P. Ringer, X.Z. Liao, Scr. Mater. 210 (2022) 114423.
[45] H.S. Oh, S.J. Kim, K. Odbadrakh, W.H. Ryu, K.N. Yoon, S. Mu, F. Kormann, Y. Ikeda, C.C. Tasan, D. Raabe, T. Egami, E.S. Park, Nat. Commun. 10 (2019) 2090.
[46] B.B. Jiang, Q. Wang, C.A. Dong, Acta Phys. Sin. 66 (2017) 026102.
[47] M.H. Tsai, J.W. Yeh, Mater. Res. Lett. 2 (2014) 107–123.
[48] E.P. George, D. Raabe, R.O. Ritchie, Nat. Rev. Mater. 4 (2019) 515–534.
[49] Q.Q. Ding, Y. Zhang, X. Chen, X.Q. Fu, D.K. Chen, S.J. Chen, L. Gu, F. Wei, H.B. Bei, Y.F. Gao, M.R. Wen, J.X. Li, Z. Zhang, T. Zhu, R.O. Ritchie, Q. Yu, Nature 574 (2019) 223–227.
[50] Y. Qian, C.Y. Jie, Y. Fang, Acta Metall. Sin. 57 (2021) 393–402.
[51] J.Y. Yan, S. Yin, M. Asta, R.O. Ritchie, J. Ding, Q. Yu, Nat. Commun. 13 (2022) 2789.
[52] Y. Wu, F. Zhang, F.S. Li, Y. Yang, J.M. Zhu, H.H. Wu, Y. Zhang, R.T. Qu, Z.F. Zhang, Z.H. Nie, Y. Ren, Y.D. Wang, X.J. Liu, H. Wang, Z.P. Lu, Mater. Horiz. 9 (2022) 804–814.
[53] F.H. Cao, Y.J. Wang, L.H. Dai, Acta Mater. 194 (2020) 283–294.
[54] J. Li, B.B. Xie, Q.F. He, B. Liu, X. Zeng, P.K. Liaw, Q.H. Fang, Y. Yang, Y. Liu, J. Mater. Sci. Technol. 120 (2022) 99–107.
[55] M.J. McCarthy, H. Zheng, D. Apelian, W.J. Bowman, H. Hahn, J. Luo, S.P. Ong, X.Q. Pan, T.J. Rupert, Phys. Rev. Mater. 5 (2021) 113601.
[56] Y. Muniandy, M.W. He, M. Eizadjou, E.P. George, J.J. Kruzic, S.P. Ringer, B. Gludovatz, Mater. Charact. 180 (2021) 111437.
[57] Y.Z. Wang, Y.J. Wang, Acta Mater. 224 (2022) 117527.
[58] S. Liu, Y.J. Wei, Extreme Mech. Lett. 11 (2017) 84–88.
[59] J. Wang, P. Jiang, F.P. Yuan, X.L. Wu, Nat. Commun. 13 (2022) 1021.
[60] T. Yang, Y.L. Zhao, Y. Tong, Z.B. Jiao, J. Wei, J.X. Cai, X.D. Han, D. Chen, A. Hu, J.J. Kai, C.T. Liu, Science 362 (2018) 933–937.
[61] B.J. Wang, Q.Q. Wang, N. Lu, X.B. Liang, B.L. Shen, J. Mater. Sci. Technol. 123 (2022) 191–200.
[62] X.L. Wu, Y.T. Zhu, Mater. Res. Lett. 5 (2017) 527–532.
[63] X.L. Wu, M.X. Yang, F.P. Yuan, G.L. Wu, Y.J. Wei, X.X. Huang, Y.T. Zhu, Proc. Natl. Acad. Sci. U. S. A. 112 (2015) 14501–14505.
[64] E.P. George, W.A. Curtin, C.C. Tasan, Acta Mater. 188 (2020) 435–474.
[65] E. Ma, Scr. Mater. 181 (2020) 127–133.
[66] Z.J. Zhang, H.W. Sheng, Z.J. Wang, B. Gludovatz, Z. Zhang, E.P. George, Q. Yu, S.X. Mao, R.O. Ritchie, Nat. Commun. 8 (2017) 14390.
[67] Z.M. Li, K.G. Pradeep, Y. Deng, D. Raabe, C.C. Tasan, Nature 534 (2016) 227–230.
[68] G. Liu, G.J. Zhang, F. Jiang, X.D. Ding, Y.J. Sun, J. Sun, E. Ma, Nat. Mater. 14 (2013) 344.
[69] X.L. Wu, F.P. Yuan, M.X. Yang, P. Jiang, C.X. Zhang, L. Chen, Y.G. Wei, E. Ma, Sci. Rep. 5 (2015) 11728.
[70] X.F. Yang, Y.Z. Xi, C.Y. He, H. Chen, X.C. Zhang, S.T. Tu, Scr. Mater. 209 (2022) 114364.
[71] C.G. Schön, Scr. Mater. 196 (2021) 113754.
[72] J.B. Seol, J.W. Bae, J.G. Kim, H. Sung, Z. Li, H.H. Lee, S.H. Shim, J.H. Jang, W.-S. Ko, S.I. Hong, H.S. Kim, Acta Mater. 194 (2020) 366–377.
[73] J. Moon, S.I. Hong, J.B. Seol, J.W. Bae, J.M. Park, H.S. Kim, Mater. Res. Lett. 7 (2019) 503–509.
[74] D.S. Zhou, Z.H. Chen, K. Ehara, K. Nitsu, K. Tanaka, H. Inui, Scr. Mater. 191 (2021) 173–178.
[75] Y. Linden, M. Pinkas, A. Munitz, L. Meshi, Scr. Mater. 139 (2017) 49–52.
[76] Y.K. Zhao, J.M. Park, J.I. Jang, U. Ramamurty, Acta Mater. 202 (2021) 124–134.
[77] T.W. Zhang, S.G. Ma, D. Zhao, Y.C. Wu, Y. Zhang, Z.H. Wang, J.W. Qiao, Int. J. Plast. 124 (2020) 226–246.
[78] Z.C. Xie, W.R. Jian, S.Z. Xu, I.J. Beyerlein, X.Q. Zhang, Z.H. Wang, X.H. Yao, Acta Mater. 221 (2021) 117380.
[79] Z.F. Lei, X.J. Liu, Y. Wu, H. Wang, S.H. Jiang, S.D. Wang, X.D. Hui, Y.D. Wu, B. Gault, P. Kontis, D. Raabe, L. Gu, Q.H. Zhang, H.W. Chen, H.T. Wang, J.B. Liu, K. An, Q.S. Zeng, T.G. Nieh, Z.P. Lu, Nature 563 (2018) 546–550.
[80] Y.Q. Bu, Y. Wu, Z.F. Lei, X.Y. Yuan, H.H. Wu, X.B. Feng, J.B. Liu, J. Ding, Y. Lu, W. Yang, Mater. Today 46 (2021) 28–34.
[81] Z. Chen, H.B. Xie, H.L. Yan, X.Y. Pang, Y.H. Wang, G.L. Wu, L.J. Zhang, H. Tang, B. Gao, B. Yang, Y.Z. Tian, H.Y. Gou, G.W. Qin, J. Mater. Sci. Technol. 126 (2022) 228–236.

[82] Z.X. Su, T. Shi, H.H. Shen, L. Jiang, L. Wu, M. Song, Z.M. Li, S. Wang, C.Y. Lu, Scr. Mater. 212 (2022) 114547.
[83] Y.W. Zhang, Y.N. Osetsky, W.J. Weber, Chem. Rev. 122 (2022) 789–829.
[84] H.J. Li, L. Zhao, Y. Yang, H.X. Zong, X.D. Ding, J. Nucl. Mater. 555 (2021) 153140.
[85] E. Ma, X.L. Wu, Nat. Commun. 10 (2019) 5623.
[86] L. Tang, F.Q. Jiang, J.S. Wrobel, B. Liu, S. Kabra, R.X. Duan, J.H. Luan, Z.B. Jiao, M.M. Attallah, B. Cai, J. Mater. Sci. Technol. 116 (2022) 103–120.
[87] A. Fantin, G.O. Lepore, A.M. Manzoni, S. Kasatikov, T. Scherb, T. Huthwelker, F. d'Acapito, G. Schumacher, Acta Mater. 193 (2020) 329–337.
[88] R. Hu, S.B. Jin, G. Sha, Prog. Mater. Sci. 123 (2022) 100854.
[89] K. Inoue, S. Yoshida, N. Tsuji, Phys. Rev. Mater. 5 (2021) 085007.
[90] L.L. Zhou, Q. Wang, J. Wang, X.F. Chen, P. Jiang, H. Zhou, F.P. Yuan, X.L. Wu, Z.Y. Cheng, E. Ma, Acta Mater. 224 (2022) 117490.
[91] D. Liu, Q. Wang, J. Wang, X.F. Chen, P. Jiang, F.P. Yuan, Z.Y. Cheng, E. Ma, X.L. Wu, Mater. Today Nano 16 (2021) 100139.
[92] K. Ohshima, D. Watanabe, Acta Crystallogr. Sect. A 29 (1973) 520–526.
[93] S.S. Sohn, D.G. Kim, Y.H. Jo, A.K. da Silva, W.J. Lu, A.J. Breen, B. Gault, D. Ponge, Acta Mater. 194 (2020) 106–117.
[94] D. Lee, M.P. Agustianingrum, N. Park, N. Tsuji, J. Alloy. Compd. 800 (2019) 372–378.
[95] D.B. Williams, C.B. Carter, Transmission Electron Microscopy: A Textbook for Materials Science, Springer, New York, 2009.
[96] G. Van Tendeloo, S. Amelinckx, Phase Transit. 67 (1998) 101–135.
[97] X.F. Chen, F.P. Yuan, H. Zhou, X.L. Wu, Mater. Res. Lett. 10 (2022) 149–155.
[98] P. Singh, A.V. Smirnov, D.D. Johnson, Phys. Rev. B 91 (2015) 224204.
[99] S. Wei, M. Stolpe, O. Gross, W. Hembree, S. Hechler, J. Bednarcik, R. Busch, P. Lucas, Acta Mater. 129 (2017) 259–267.
[100] S.H. Kayani, S. Park, J.G. Kim, J.B. Seol, H. Sung, Scr. Mater. 213 (2022) 114642.
[101] F.X. Zhang, S. Zhao, K. Jin, H. Xue, G. Velisa, H. Bei, R. Huang, J.Y.P. Ko, D.C. Pagan, J.C. Neuefeind, W.J. Weber, Y. Zhang, Phys. Rev. Lett. 118 (2017) 205501.
[102] M. Widom, W.P. Huhn, S. Maiti, W. Steurer, Metall. Mater. Trans. A-Phys. Metall. Mater. Sci. 45 (2013) 196–200.
[103] A. Tamm, A. Aabloo, M. Klintenberg, M. Stocks, A. Caro, Acta Mater. 99 (2015) 307–312.
[104] L.J. Santodonato, Y. Zhang, M. Feygenson, C.M. Parish, M.C. Gao, R.J. Weber, J.C. Neuefeind, Z. Tang, P.K. Liaw, Nat. Commun. 6 (2015) 5964.
[105] A. Fernández-Caballero, J.S. Wróbel, P.M. Mummery, D. Nguyen-Manh, J. Phase Equilib. Diffus. 38 (2017) 391–403.
[106] L. Koch, F. Granberg, T. Brink, D. Utt, K. Albe, F. Djurabekova, K. Nordlund, J. Appl. Phys. 122 (2017) 105106.
[107] Q.F. He, P.H. Tang, H.A. Chen, S. Lan, J.G. Wang, J.H. Luan, M. Du, Y. Liu, C.T. Liu, C.W. Pao, Y. Yang, Acta Mater. 216 (2021) 117140.
[108] Y. Rao, W.A. Curtin, Acta Mater. 226 (2022) 117621.
[109] M. Mizuno, K. Sugita, H. Araki, Results Phys. 34 (2022) 105285.
[110] T. Kostiuchenko, A.V. Ruban, J. Neugebauer, A. Shapeev, F. Körmann, Phys. Rev. Mater. 4 (2020) 113802.02.
[111] Z.Q. Shen, J.P. Du, S.H. Shinzato, Y.J. Sato, P.J. Yu, S. Ogata, Comput. Mater. Sci. 198 (2021) 110670.
[112] B.Z. Zhang, J. Ding, E. Ma, Appl. Phys. Lett. 119 (2021) 201908.
[113] E.A. Meshkov, I.I. Novoselov, A.V. Shapeev, A.V. Yanilkin, Intermetallics 112 (2019) 106542.
[114] X.S. Huang, L.H. Liu, X.B. Duan, W.B. Liao, J.J. Huang, H.B. Sun, C.Y. Yu, Mater. Des. 202 (2021) 109560.
[115] X.L. Wu, Y.T. Zhu, K. Lu, Scr. Mater. 186 (2020) 321–325.
[116] X.L. Wu, Y.T. Zhu, MRS Bull. 46 (2021) 244–249.
[117] B.B. He, B. Hu, H.W. Yen, G.J. Cheng, Z.K. Wang, H.W. Luo, M.X. Huang, R.O. Ritchie, Science 357 (2017) 1029–1032.